Heliyon 10 (2024) e37802

Contents lists available at ScienceDirect

Heliyon

journal homepage: www.cell.com/heliyon

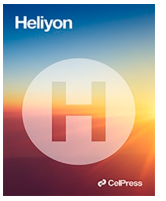

Research article

Synthesis, characterization, and evaluation of antibacterial and antifungal activities of CuO-ZnO-Co_3O_4 nanocomposites

Shadha Nasser Aziz [a,c,*], A.M. Abdulwahab [b,**], Thana Shuga Aldeen [a], Dheyazan Mohammed Ali Alqabili [d]

[a] Physics Department, Faculty of Science, Sana'a University, Sana'a, Yemen
[b] Physics Department, Faculty of Applied Science, Thamar University, Dhamar 87246, Yemen
[c] Al-Darb Community College, Dhamar, Yemen
[d] Department of public health and zoonoses, Faculty of agriculture and veterinary Thamar University, Dhamar 87246, Yemen

ARTICLE INFO

Keywords:
Co-precipitation
Nanocomposites
(TEM)
X-ray diffraction
Optical bandgap, antibacterial and antifungals activity

ABSTRACT

The co-precipitation method was used to prepare CuO, ZnO, Co_3O_4 nanoparticles and CuO-ZnO-Co_3O_4 nanocomposite. The structural, morphological, and optical properties of the prepared samples were studied using X-ray diffraction (XRD), total reflection X-ray fluorescence (TXRF), transmission electron microscopy (TEM), selected area electron diffraction (SAED), diffuse reflectance spectroscopy (DRS), and zeta potential. XRD analysis revealed that the crystal structures of CuO, ZnO, and Co_3O_4 nanoparticles are monoclinic, hexagonal, and cubic, with average crystallite sizes of 30.8 nm, 31.8 nm, and 32.8 nm, respectively. For CuO-ZnO-Co_3O_4 nanocomposites, the corresponding sizes were 24.9 nm, 13.6 nm, and 16.1 nm. The optical bandgaps of CuO, ZnO, Co_3O_4 nanoparticles, and CuO-ZnO-Co_3O_4 nanocomposites were 1.5 eV, 3.14 eV, 1.2 eV, and 1.3 eV, respectively. In this study, the antibacterial activity of CuO-ZnO-Co_3O_4 nanocomposite against Gram-negative bacteria (*E. coli, Klebsiella, pseudomonas, and Salmonella*) and Gram-positive bacteria (*Staphylococcus aureus*) was investigated and compared with the antibiotic *Azithromycin*. In addition, the effect of the nanocomposite on fungi was studied and compared with the antifungal *Mystatin*.

1. Introduction

Mixed metal oxide (MMO) nanocomposites are made by combining several metal oxides with nanometer-sized particles. Due to their newly discovered and significantly enhanced physicochemical and biological properties as a result of their size reduction, metal oxide nanoparticles and other nanomaterials have garnered a great deal of scientific attention recently [1]. It has some properties, including thermal, optical, electrical, photocatalytic, and structural characteristics. Nanometer-scale mixing of more than one oxide results in the formation of nanoparticles, whose properties depend on the relative concentrations of the individual oxide components in the mixture. Applications for the nanocomposites could include fuel cells, battery components, photovoltaic devices, UV detectors, gas sensors, and solar cells. Increases in carrier lifetime, charge transfer capacity, charge separation efficiency, magnetic property at room temperature, and biomedical applications may be caused by metal-oxygen and metal-metal interfaces in mixed metal oxides [2–5].

* Corresponding author. Physics Department, Faculty of Science, Sana'a University, Sana'a, Yemen.
** Corresponding author.
E-mail addresses: Shd.Aziz@su.edu.ye (S.N. Aziz), abduhabdulwahab@yahoo.com (A.M. Abdulwahab).

https://doi.org/10.1016/j.heliyon.2024.e37802
Received 19 March 2024; Received in revised form 9 September 2024; Accepted 10 September 2024
Available online 11 September 2024

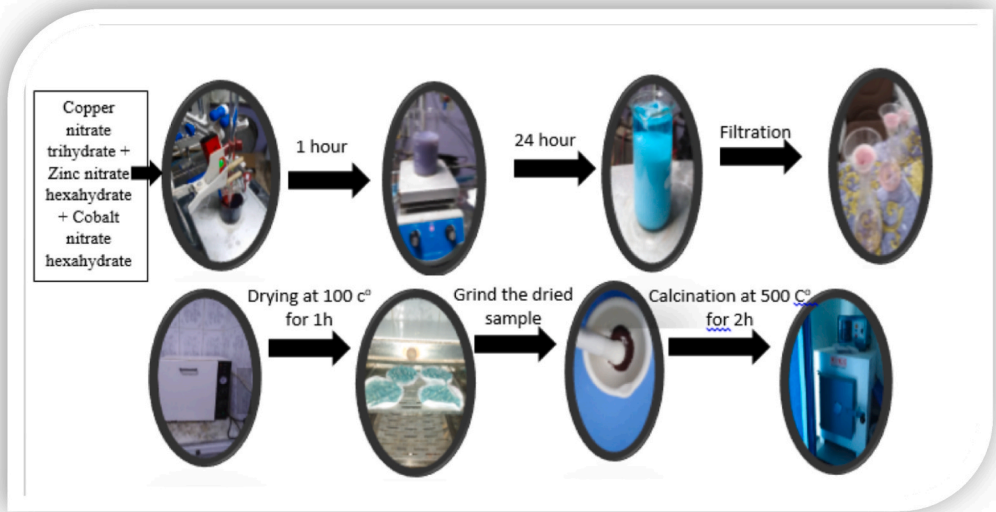

Fig. 1. Representation of the synthesis processes of CuO, ZnO,Co_3O_4 nanoparticals and CuO-ZnO- Co_3O_4 nanocomposite.

MMO nanocomposites were prepared using common methods such as Sol- Gel [6], mechanical grinding [7], hydrothermal technique [8], Microwave-assisted [9], solid-state reaction [10], and co-precipitation method [11]. The co-precipitation method is used due to its simplicity, affordability, efficacy, room temperature growth, fast, and low cost [12].

It has been demonstrated that CuO nanoparticle cause bacterial cell membrane disruption, which results in cell death. Reactive oxygen species (ROS) and copper ions are released, resulting in oxidative stress and damage to cellular components. Furthermore, CuO nanoparticle have shown a strong antifungal effect. According to studies, they are beneficial in biological and agricultural applications because they prevent the growth of fungi such as *Fusarium Oxysporum* and *Botrytis cinerea* [13,14].

It has been discovered that ZnO nanoparticle work well against a variety of bacterial strains, including gram-positive and gram-negative bacteria. Their process includes breaking down bacterial cell membranes and producing ROS. In addition, ZnO nanoparticle work well against *Aspergillus Niger* and *Candida albicans*. They prevent spore germination and harm fungal cells structurally [15–18].

By causing oxidative stress and rupturing bacterial cell membranes, Co_3O_4 nanoparticle have proven effective against a variety of bacterial strains (RSC Publishing) (Frontiers). This results in cell death. Along with though studies on Co_3O_4 nanoparticle are not as comprehensive as those on CuO and ZnO, research suggests that they can prevent the growth of fungi. They have demonstrated efficacy in combating pathogens such as *Fusarium Oxysporum*, underscoring their potential for use in biological applications [19,20].

Gram-positive and Gram-negative bacterial strains are regarded as a significant public health issue as infectious diseases become more prevalent globally. Especially with the emergence of antibiotic-resistant strains of bacteria [21]. Recently, antimicrobial resistance has increased globally, particularly for *Candida* infections. Most of the antifungal drugs used for treating candidiasis became resistant to most *Candida* species.

In this way, nanomaterials are used as antibacterial agents due to their surface, size, and structure properties. Metal oxide nanoparticles such as CuO, ZnO, and Co_3O_4 are excellent antibacterial agents that can be used to treat many infections caused by bacteria like *Escherichia coli, Klebsiella pneumoniae, Staphylococcus aureus*, and *Streptococcus pyrogens* [22–26]. When three metal oxides are combined in a ternary system, new and improved characteristics can be produced, like stronger thermal stability, better electrical conductivity, and increased catalytic activity [27]. Previous studies have demonstrated the antibacterial properties of ternary metal oxide nanocomposites. Dias et al. have evaluated the antibacterial and antifungal activity of CuO-MgO-ZnO and CuO-Co_3O_4-CeO_2 trioxides synthesized via precipitation [28]. Kannan et al. have described the photocatalytic and antimicrobial properties of microwave synthesized CdO-CuO-ZnO nanocomposite [29]. Antibacterial activity of the CuO-NiO-ZnO mixed metal oxide has been reported by Alam et al. [30].

As far as our knowledge is concerned, the papers on these nanocomposites are scarce and their applications have not received enough studies, so the reason for the choice and coupling of these metals. The structural, morphological, and optical properties of CuO, ZnO, and Co_3O_4 nanoparticles, and CuO-ZnO-Co_3O_4 nanocomposite were investigated. Also, antibacterial and antifungal activity were evaluated and compared between five different bacterial species and *candida* as a useful application of the prepared nanoparticles and nanocomposite.

2. Experimental details

2.1. Materials

Copper nitrate trihydrate ($Cu(NO_3)_2.3H_2O$) (98 %) (HIMEDIA), Zinc nitrate hexahydrate ($Zn(NO_3)_2.6H_2O$) (99 %) (HIMEDIA), Cobalt nitrate hexahydrate ($Co(NO_3)_2.6H_2O$) (98 %) (HIMEDIA), Sodium hydroxid NaOH (98 %) (HIMEDIA), and Distilled Water (DW) were used in this work.

2.2. Preparation of CuO, ZnO, and Co_3O_4 nanoparticles

0.03*M of* ($Cu(NO_3)_2.3H_2O$) was dissolved in 100 mL of distilled water under constant stirring for 10 min. 0.1 M NaOH is added dropwise to the solution to adjust its pH value to 7, and it is stirred for 1h at ambient temperature to obtain the solution. The final solutions are kept in an airtight container overnight. The obtained precipitate is washed with distilled water several times, dried at 100 °C for 1 h, then ground using a mortar and a pestle to get a fine powder. Finally, the powder is annealed at 500 °C for 2 h to obtain the nanoparticles. These steps were repeated for other tow oxides (ZnO and Co_3O_4) with ($Zn(NO_3)_2.6H_2O$) and ($Co(NO_3)_2.6H_2O$) as starting materials (see Fig. 1).

2.3. Synthesis of CuO-ZnO-Co_3O_4 nanocomposite

To prepare (CuO-ZnO-Co_3O_4) nanocomposite, 0.03M of copper nitrate, zinc nitrate, and cobalt nitrate with molar ratios (1:1:1) were dissolved in 300 mL of distilled water under constant stirring for 10 min. The nanocomposite was then prepared using the same procedure as for the synthesis of CuO, ZnO, and Co_3O_4

2.4. Characterizations

The structural characteristics of the prepared CuO, ZnO, Co_3O_4 nanoparticles, and CuO-ZnO-Co_3O_4 nanocomposite were examined using XRD (XD-2 X-ray diffractometer using CuK_α ($\lambda = 1.54$ Å) at 36 kV and 20 mA, China). The concentrations of each element in the samples were measured using a TXRF (xrf, s8 tiger, German) in the Yemeni Geological Survey and Minerals Resources Board. The nanoparticle size was determined using a TEM (JEM-2100, Japan). The size of the TEM images was evaluated using ImageJ software. In the Egypt National Research Centre (DRS), Model JASCO (V-750, Japan) was used to measure the transformation of the reflectance spectra. For zeta potential and particle size, 1 mg of each sample was dispersed in 1 mL of deionized water, then sonicated for 30 min and diluted 10X with deionized water. By utilizing a particle size analyzer called Dynamic Light Scattering (DLS) (Zetasizer Nano ZN, Malvern Panalytical Ltd., United Kingdom) at a fixed angle of 173° at 25 °C, the prepared particles were examined for their particle size and size distribution in terms of the average volume diameters and polydispersity index. Each sample was examined three times. The zeta potential was calculated using the same tools.

2.5. Antibacterial and antifungal activity

2.5.1. Preparation of standardized suspension

A few colonies of similar morphology from each bacteria isolate were transferred, utilizing a sterile loop,to a tube containing 5 ml of sterile 0.85 % physiological saline. The addition of sterile saline or other colonies to the tube was applied until the turbidity was adjusted to match 0.5 McFarland standard tubes using adequate light [31].

The antibacterial effectiveness of the CuO, ZnO, Co_3O_4 nanoparticles, and CuO-ZnO-Co_3O_4 nanocomposite were evaluated against five bacterial pathogens using the agar-well diffusion method. Bacterial colonies were cultured in nutrient broth at 37 °C for 24 h with gram-positive (*Staphylococcus*) and gram-negative (*E. coli, Klebsiella, Pseudomonas, and Salmonella*) organisms. 15 mL of Mueller-Hinton agar was added to Petri dishes and allowed to set up. Five different concentrations of each nanocomposite (1, 2, 4, 8, and 16) in addition to azithromycin were added as a control immediately to the plates [32]. The plates were then heated at 37 °C for 24 h of incubation. After incubation, the degree of sensitivity was determined by measuring the easily visible and clear zone of inhibition of growth produced by the diffusion of the antimicrobial agent from the wells into the surrounding medium. The diameter of the inhibition zone for each antimicrobial agent was measured and interpreted according to Poirel [33].

The only pure colony of yeast was selected using a sterile swab dipped in sterile tween 80. After being vortexed, this was suspended in 3–4 mL of sterile normal saline. A 0.5 McFarland standard was set for the suspension's turbidity. In a similar manner, the pure colony was swabbed to prepare the inoculum for mold. This suspension was then vortexed in 3–4 mL of sterile normal saline. A 0.5 McFarland standard was set for the suspension turbidity [34].

Candida was utilized to assess the antifungal activity of CuO, ZnO, Co_3O_4 nanoparticles, and CuO-ZnO-Co_3O_4 nanocomposite. Petri dishes were filled with 15 mL of Sabouraud agar, which was then allowed to set. Five samples of antifungal nanocomposites (*Mystatin*) were then immediately added to the plates. Following that, it was left out at room temperature for 24–48 h. The size of the inhibition zone was then measured.

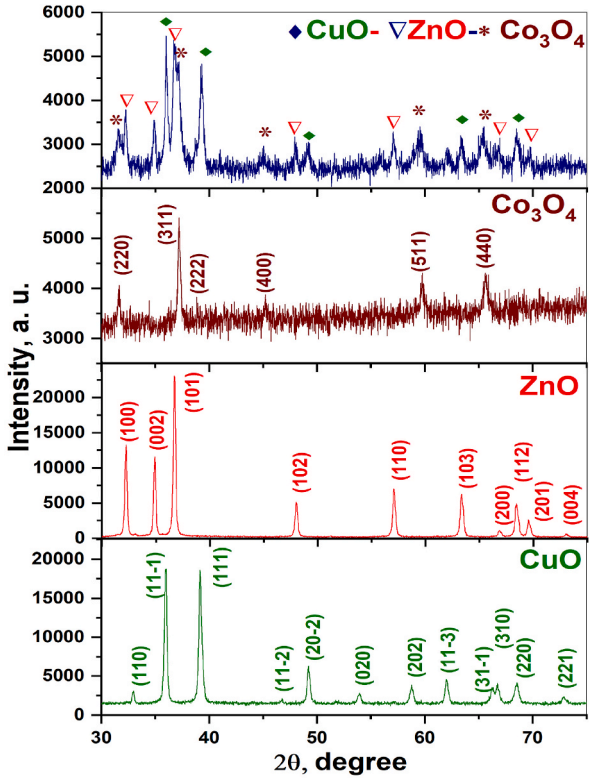

Fig. 2. XRD patterns of CuO, ZnO, Co_3O_4 nanoparticals and CuO–ZnO-Co_3O_4 nanocomposite.

Table 1
The Peak positions and corresponding Miller indices for CuO, ZnO, Co_3O_4 nanoparticles and CuO-ZnO-Co_3O_4 nanocomposite.

CuO		ZnO		Co_3O_4		CuO-ZnO-Co_3O_4					
						CuO		ZnO		Co_3O_4	
2θ	(*hkl*)	2θ	(*hkl*)	2θ	(*hkl*)	2θ	(*hkl*)	2θ	(*hkl*)	2θ	(*hkl*)
32.26	(110)	32.1	(100)	31.04	(220)	–	–	32.3	(100)	31.46	(220)
35.88	(11 $\bar{1}$)	34.8	(200)	36.6	(311)	35.99	(11 $\bar{1}$)	34.6	(002)	–	–
38.44	(111)	36.7	(101)	38.42	(222)	38.76	(111)	36.8	(101)	39.26	(222)
45.98	(11 $\bar{2}$)	48	(102)	44.72	(400)	–	–	47.9	(102)	44.99	(400)
49.2	(20 $\bar{2}$)	57.1	(110)	59.479	(511)	49.22	(20 $\bar{2}$)	56.9	(110)	59.59	(511)
53.44	(020)	63.4	(103)	64.94	(440)	–	–	63.3	(103)	65.26	(440)
58.74	(202)	66.2	(200)	–	–	–	–	67.04	(200)	–	–
61.66	(11 $\bar{3}$)	68.6	(112)	–	–	61.8	(11 $\bar{3}$)	–	–	–	–
66.17	(31-1)	69.7	(201)	–	–	–	–	–	–	–	–
66.4	(310)	73.2	(400)	–	–	–	–	–	–	–	–
68.62	(220)	–	–	–	–	68.66	(220)	–	–	–	–
73.06	(221)	–	–	–	–	–	–	–	–	–	–

3. Results and discussion

3.1. X-ray diffraction (XRD)

The XRD patterns of CuO- ZnO- Co_3O_4 nanocomposite along with pure CuO, ZnO, and Co_3O_4 nanoparticles are presented in Fig. 2. The XRD pattern of CuO- ZnO- Co_3O_4 nanocomposite is in good agreement with standard JCPDS cards no:00-048-1548 (CuO) [35], JCPDS cards no:00-001-1136 (ZnO) [36], and JCPDS cards no: 00-042-1467 (Co_3O_4) [37], confirming the existence of three phases in the single matrix. The observed diffraction patterns of nanocomposite demonstrated that CuO has a monoclinic structure, ZnO has a hexagonal structure, and Co_3O_4 has a cubic structure. Peak positions and corresponding Miller indices for the nanoparticles and nanocomposite are listed in Table 1. There was no impurity peak noticed in the XRD pattern, confirming the successful growth of pure CuO- ZnO- Co_3O_4 nanocomposite.

The intensity of CuO and ZnO peaks are higher than that of Co_3O_4 in the CuO-ZnO-Co_3O_4 nanocomposite pattern (Fig. 2). This is

Table 2
The values of D and ε for CuO, ZnO, Co_3O_4 nanoparticles and CuO- ZnO-Co_3O_4 nanocomposite determined by XRD analysis.

Sample		a (A^0)	b (A^0)	c (A^0)	**D(*nm*)**	ε
Metal oxides	CuO	4.6	3.4	5.1	30.76	0.004058
	ZnO	3.2	–	5.1	31.79	0.0039747
	Co_3O_4	8.1	–	–	32.8	0.00644328
CuO-ZnO-Co_3O_4	CuO	4.7	3.4	5.1	30.23	0.004073
Mixed metal oxides	ZnO	3.23	–	5.2	26.66	0.00474
	Co_3O_4	8.01	–	–	26.73	0.003579

Table 3
TXRF analysis of CdO-CuO-Co_3O_4 nanocomposite.

Compound	Wt%	Elemental	Wt%
CuO	46.83 %	Cu	37.52 %
ZnO	30.92 %	Zn	24.67 %
Co_3O_4	21.87 %	Co	16.83 %
–	–	O	20.60 %
P, S, Ca, Fe, Si, etc	0.38 %	P, S, Ca, Fe, Si, etc	0.38 %

due to the relatively lower CuO contents, as confirmed by elemental analysis. Additionally, a slight deviation of peak positions in the nanocomposite may be because of interaction between CuO, ZnO, and Co_3O_4 phases.

The average crystallite sizes of CuO, ZnO, Co_3O_4 nanoparticles, and CuO-ZnO-Co_3O_4 nanocomposite were calculated using Debye-Scherrer's formula Eq. (1) [38,39].

$$D = (0.9\ \lambda)/(\beta\ \mathrm{CoS}\ \theta) \tag{1}$$

Where λ is the wavelength of X-ray used, β is the full-width at half maximum intensity (FWHM) (in radian), θ is the diffraction angle. The lattice constant "a, b,c" determine for all prepare nanocomposite from high intense diffraction peak of (*hkl*) plane using the following Bragg's equation for cubic structure Eq. (2) [40]

$$\frac{1}{d^2} = \left[\frac{h^2 + k^2 + l^2}{a^2}\right] \tag{2}$$

Hexagonal structure Eq.3 [41].

$$\frac{1}{d^2} = \frac{4}{3}\left[\frac{h^2 + hk + k^2}{a^2}\right] + \frac{l^2}{c^2} \tag{3}$$

And monoclinic structure Eq. (4) [42]

$$\frac{1}{d^2} = \frac{1}{sin^2\,\beta}\left[\frac{h^2}{a^2} + \frac{k^2\,sin^2\,\beta}{b^2} + \frac{l^2}{c^2} - \frac{2hlcos\beta}{ac}\right] \tag{4}$$

The micro-strain was determined ~~by~~ using Eq. (4), [42]. The calculated values of D and ε are summarized in Table 2.

There is a slight increase in the lattice parameters of CuO and ZnO in the nanocomposite, while that of Co_3O_4 decreased compared with nanoparticles. The crystallite sizes of individual CuO, ZnO, Co_3O_4 nanoparticles and CuO-ZnO-Co_3O_4 nanocomposite are shown in Table 2. The decrease in the crystallite sizes of ZnO and Co_3O_4 in the nanocomposite infers that CuO is the dominant phase in the nanocomposite, The result was accepted by Ishfaq et al. [43]. The decrease in crystalline size is often associated with a higher density of defects and dislocations within the crystal lattice. These defects contribute to microstrain by disrupting the regular atomic arrangement. The micro-strain (ε) of CuO and ZnO in the nanocomposite increased when compared to their values as nanoparticles. Due to the crystallite size decreased in the nanocomposite, the antibacterial and photocatalytic activity increased. This result has very good agreement with previous work [4,44].

3.2. Elemental analysis

Table 3 shows the results of the elemental composition and oxide composition of CuO-ZnO- Co_3O_4 nanocomposite carried out by TXRF. The results clearly indicated the existence of Cu, Zn, Co and O as elements and CuO, ZnO, Co_3O_4 as oxides.

3.3. TEM analysis of CuO-ZnO-Co_3O_4

The size and shape of the synthesized nanoparticles and nanocomposite were characterized utilizing TEM (Fig. 3a) shows TEM images of CuO, ZnO, Co_3O_4 nanoparticles and CuO-ZnO-Co_3O_4 nanocomposite. As can be seen, CuO, ZnO, Co_3O_4 nanoparticles and

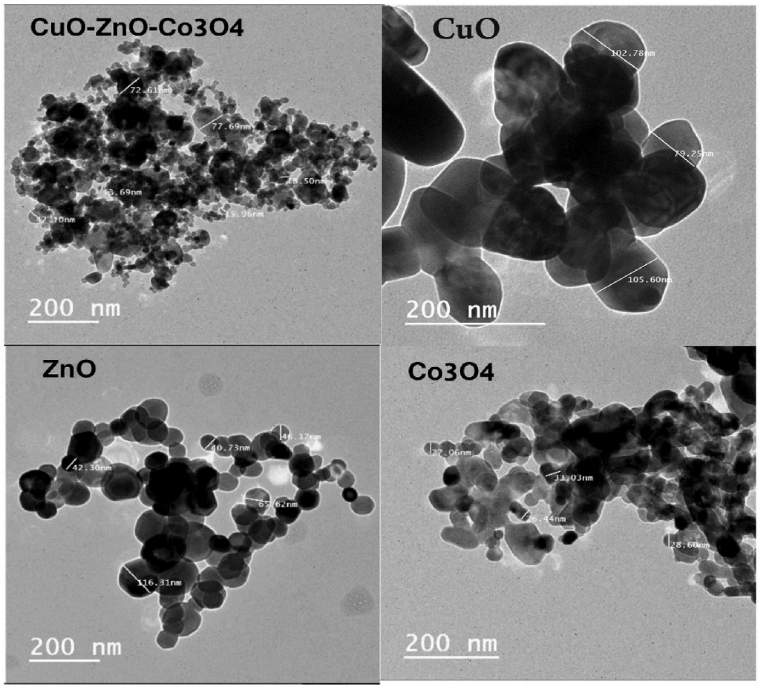

a

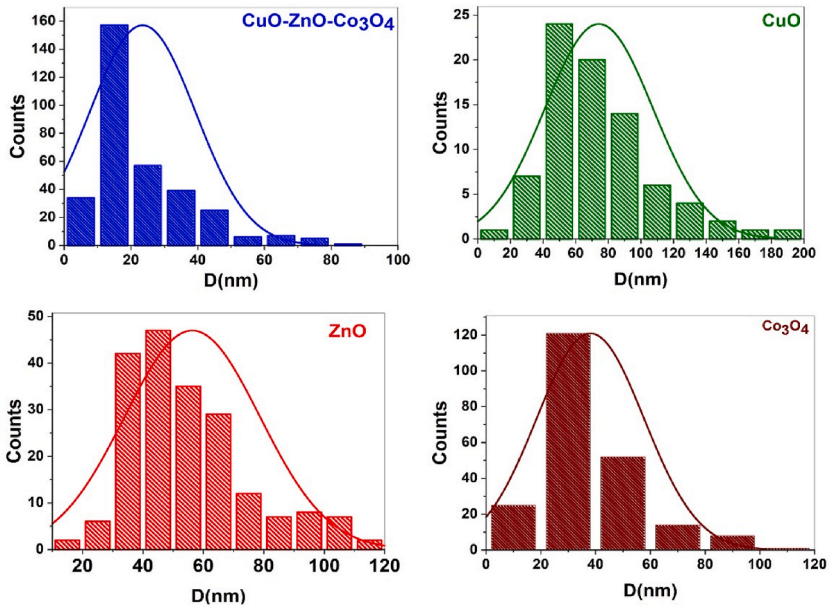

b

Fig. 3. a. TEM image of CuO,ZnO,Co_3O_4 nanoparticals and CuO-ZnO-Co_3O_4 nanocomposite. fig. 03, bparticle size distribution of CuO,ZnO,Co_3O_4 nanoparticals and CuO-ZnO-Co_3O_4 nanocomposite. fig. 03,c.SAED crystal ring patterns obtained for the CuO,ZnO,Co_3O_4 nanoparticals and CuO-ZnO-Co_3O_4 nanocomposite.

CuO-ZnO-Co_3O_4 nanocomposite have spherical shapes. The image-J program was used to calculate their particle sizes, and the histogram graph was plotted in (Fig. 3b). The particle sizes of CuO, ZnO, Co_3O_4 nanoparticles and CuO-ZnO-Co_3O_4 nanocomposite are 70.7 nm, 51.8 nm, 33.4 nm, and 18.1 nm respectively. As is clear from (Fig. 3) the circular fringes in SAED patterns indicate the polycrystalline nature of the samples, and the diffraction rings matched with the XRD d-spacing of CuO, ZnO, Co_3O_4 nanoparticles and

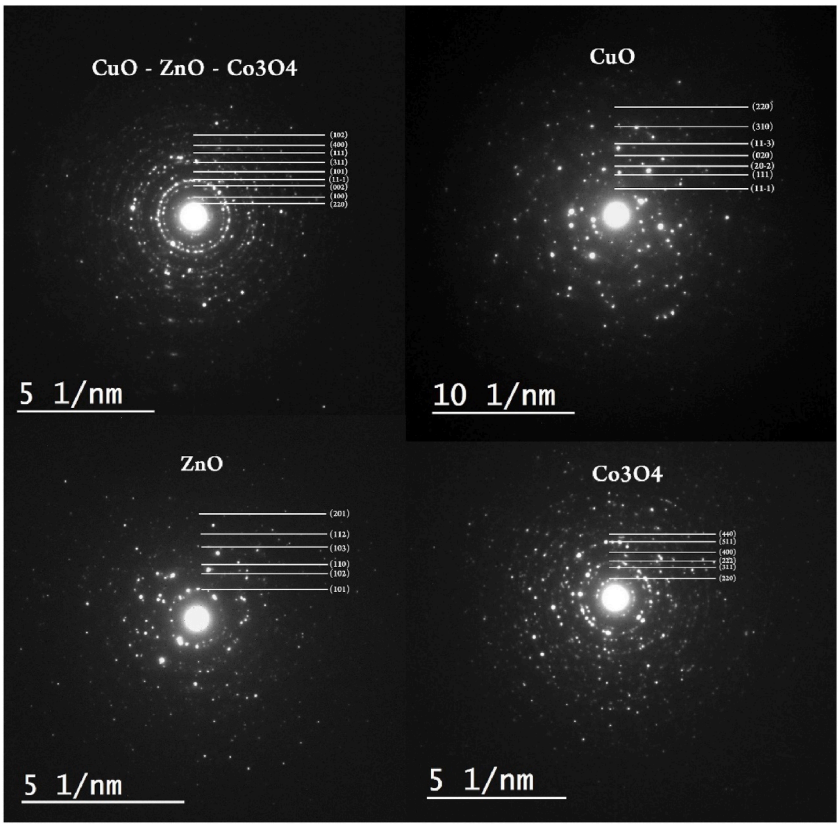

Fig. 3. (*continued*).

Table 4
Zeta Potential and Particle size for the CuO,ZnO, Co_3O_4 nanoparticles and CuO-ZnO-Co_3O_4 nanocomposite.

Samples	**Zeta Potential (*mV*)**	**Size Distribution (*nm*)**
CuO	−21.7	933
ZnO	2.78	634
Co_3O_4	12	516
CuO-ZnO-Co_3O_4	14.9	978

CuO-ZnO-Co_3O_4 nanocomposite. The TEM results are in good agreement with the XRD results, which showed a decrease in the crystalline size of nanocomposite compared to nanoparticles.

3.4. Zeta potential and size distribution

It is essential to characterize the behavior of NPs in an aqueous state before their biological studies. The dynamic light scattering (DLS) technique is a widely used and effective method for determining the size of particles in a colloidal solution. The size of NPs is an important characteristic for the use of nanoparticles in several fields, particularly the biomedical field. Zeta potential determination is an important technique to estimate the surface charge of nanoparticles, which is helpful in the determination of the colloidal stability of NPs [30].

Nanoparticles that possess zeta potentials of more than +20 mV or less than −20 mV are considered stable colloidal suspension systems that prevents nanoparticles aggregation. On the other hand, nanoparticles with zeta potential values that fall between −30 mV and +30 mV indicate poor colloidal stability and are likely to undergo flocculation, agglomeration, or aggregation [45–47]. The stability behavior of synthesized CuO, ZnO,Co_3O_4 nanoparticles, and CuO-ZnO-Co_3O_4 nanocomposite have been examined using zeta potential and size distribution. As shown in Table 4 and Fig. 4.

The CuO, ZnO, Co_3O_4 nanoparticles, and CuO-ZnO-Co_3O_4 nanocomposite had a mean size distribution with diameters between 500 and 980 nm. Our analysis showed that the average particle size reported by DLS was higher than the one obtained by TEM. The disparity seen between TEM and DLS aligns with many additional investigations that documented the synthesis of diverse NPs [48]. The difference in size between the nanoparticles as measured by DLS and TEM is due to the swelling of CuO, ZnO, Co_3O_4 nanoparticles,

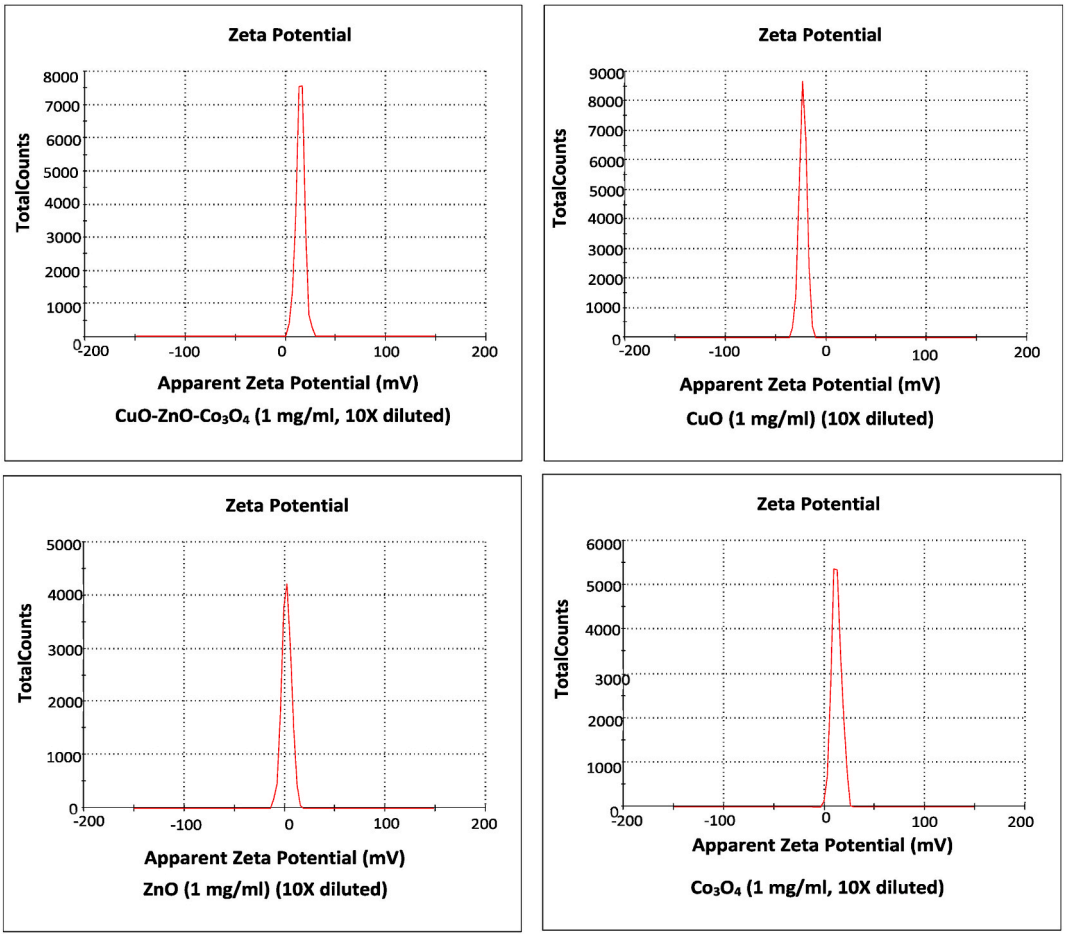

Fig. 4. Zeta Potential Distribution the CuO,ZnO,Co_3O_4 nanoparticals and CuO-ZnO-Co_3O_4 nanocomposite.

and CuO-ZnO-Co_3O_4 in an aqueous medium. The zeta potentials of the CuO, ZnO, Co_3O_4 nanoparticles and CuO-ZnO-Co_3O_4 nanocomposite were determined to be −21.7, 2.78, 12, and 14.9 mV respectively. The CuO nanoparticles are more stable than Co_3O_4 nanoparticles and CuO-ZnO-Co_3O_4 nanocomposite, while ZnO has poor stability. This result agrees with Ola N Hussen [49].

3.5. Optical bandgap energy

Diffuse reflectance spectroscopy was utilized to study the optical properties of CuO, ZnO, Co_3O_4 nanoparticles and CuO-ZnO-Co_3O_4 nanocomposite materials that were synthesized. Fig. 5 shows the sample's reflectance spectrum as a function of wavelength (a) in the spectral range 400–700 nm. The results demonstrate the reflectance spectrum. Utilizing the Kubelka-Munk equation, the measured reflectance was converted to absorbance [50] (see Fig. 6).

$$F(R) = \frac{(1-R)^2}{2R} \tag{6}$$

Where R is the diffuse reflectance (%) and F(R) is the Kubelka-Munk function corresponding to the absorbance. The modified K-M equation was used to determine the material's bandgap energy (E_g) and the type of optical transition between the valence band (VB) and conduction band (CB) [51]:

$$(F(R)h\upsilon) = A\left(E - E_g\right)^n \tag{7}$$

The exponent factor n is related to the type of the optical transition and has a value of 1/2 for the direct allowed band gap, and the transition probability can be determined by the A constant. ($E = h\upsilon$) is the photon energy. Plotting $\left((F(R)\,h\,\upsilon)^{\frac{1}{n}}\right)$ versus $E(eV)$ and extrapolating the linear portion of the plot up to $(F(R)\,h\,\upsilon)^{1/n} = 0$) can be used to estimate the E_g of materials [50]. The type of transition is determined by the best linear fit using various values of n; this kind of representation is called a Tauc model. shows the Tauc plot obtained for the as-prepared CuO, ZnO, Co_3O_4 nanoparticles, and CuO-ZnO-Co_3O_4 nanocomposite. Table 5 shows the

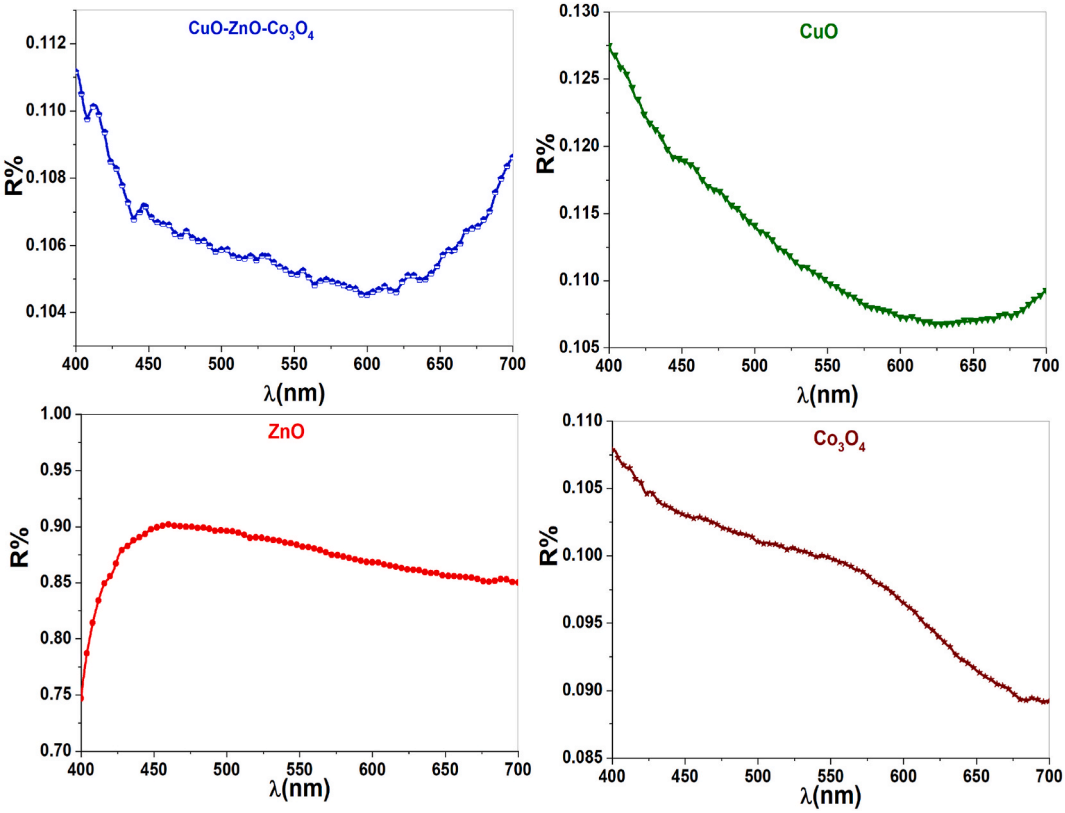

Fig. 5. Diffuse reflectance spectrum (R%) of theCuO,ZnO,Co_3O_4 nanoparticals and CuO-ZnO-Co_3O_4 nanocomposite.

obtained band gap E_g values of prepared samples.

The bandgap value of CuO- ZnO- Co_3O_4 nanocomposite is close to that of CuO and Co_3O_4 (NPs). The shift in the bandgap energy of the nanocomposite compared to the individual metal oxides may be caused by new energy states that form at the interfaces of the several metal oxides. This may cause the bandgap energy and the electrical structure to change. Co_3O_4 (NP) has two bandgaps at 1.4 eV and 1.16 eV; the presence of Co(III) centers in Co_3O_4 gives rise to a sub-band located inside the energy gap. Hence, E_{g1} corresponds to the onset of $O(-II) \longrightarrow Co(III)$ excitations, while E_{g2} is the "true'' energy gap corresponding to inter-band transitions (basic optical band gap energy, or valence to conduction band excitation) [52]. The optical band gap of CuO-ZnO- Co_3O_4 nanocomposite is lower than that of nanoparticles. The band gap value of nanocomposite (1.3 eV) falls within the range of a narrow band gap semiconductor. We can compare the particle size effect with the band gap only for semiconductors that have a size in the quantum dot (QD) [53,54]. Materials with such band gaps can have potential applications in fields such as photovoltaic, photocatalysis and sensors.

3.6. Antibacterial and antifungal activities

The antibacterial activity of the CuO, ZnO, Co_3O_4, and CuO-ZnO-Co_3O_4 nanocomposite was evaluated against *E. coli, Klebsiella, pseudomonas, salmonella, and Staphylococcus* bacterial strains by a disc different approach and is shown in (Fig. 7). The nanoparticles and nanocomposite were studied for five different concentrations: 1, 2, 4, 8, and 16 mg; these values were compared with antibacterial (*Azithromycin (*30 mg)).

Fig. 8 shows that the bacteria are sensitive to the CuO-ZnO-Co_3O_4 (16 mg) nanocomposite. The inhibition zones are measured as follows: 12, 15, 13, 13, and 14 mm, respectively; the weight of (8 mg) was 11, 9, 12, 9, and 12 mm respectively; and the weight of (4 mg) was 7, 9, 7, 8, and 8 mm, respectively. Its sensitivity to the ZnO (16 mg) nanoparticles was 8, 10, 13, 9, and 14 mm, respectively. The sensitivity of bacteria to *azithromycin* (30 mg) was 15, 18, 21, 18, and 14 mm, respectively. There is no effect of the Co_3O_4 and CuO nanocomposite.

The antifungal screening was performed on *candida*, using *Mystatin* as a reference (Fig. 9). Fig. 10 shows that the *candida* are sensitive to the CuO-ZnO-Co_3O_4 nanocomposite (1, 2, 4, 8, and16 mg); the inhibition zones are measured as follows: 8, 8,9,12 and 14 mm, respectively. For CuO NPs with (1,2,4,8, and 16 mg) concentrations, the inhibition zones are measured as follows: 0,0,7,14, and 18 mm respectively, and ZnO NPs (1,2,4,8, and 16 mg) concentrations, the inhibition zones are measured as follows: 11,0,0,9, and 10 mm respectively. There is no effect on the Co_3O_4 NPs. The sensitivity of *candida* to *Mystatin* (30 mg) was 12 mm. Nanocomposites have improved nanoparticles in antibacterial and antifungal Activities as confirmed by result of XRD and TEM.

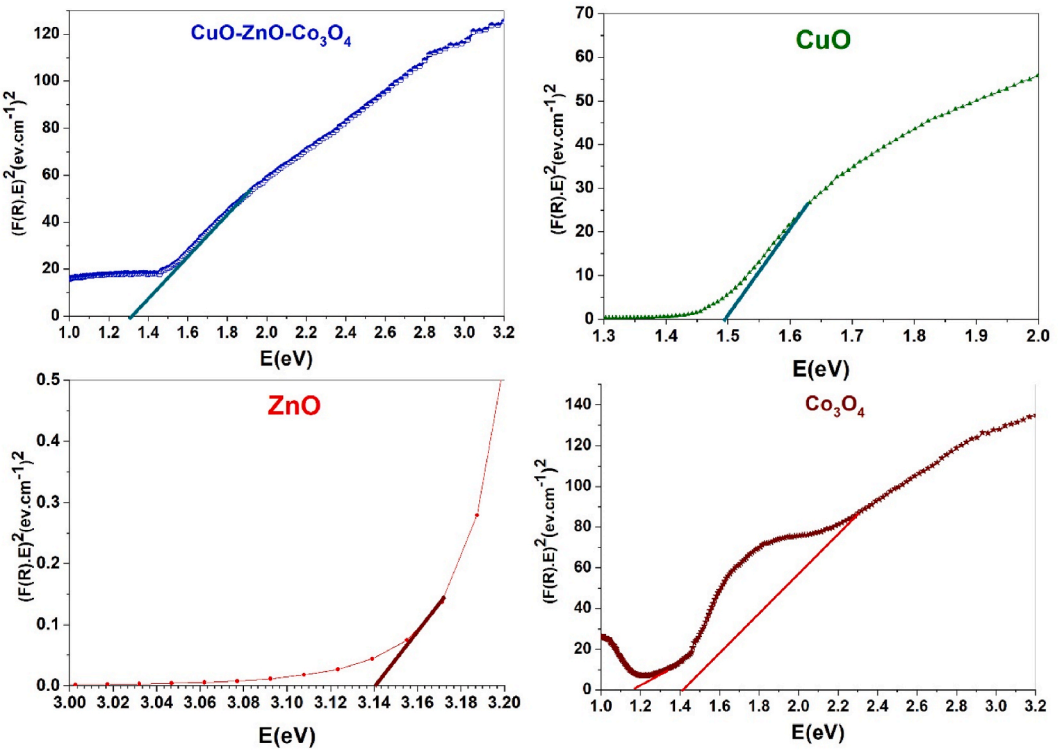

Fig. 6. The plot of $(F(R)h\nu)^2$ vs $E(eV)$ for direct band gap.

Table 5
Optical bandgap energy values of prepared sample.

Sample	$E_g(eV)$
CuO	1.5
ZnO	3.14
Co_3O_4	1.16 &1.4
CuO-ZnO-Co_3O_4	1.3

Reactive oxygen species (ROS) photo generation on the surface of metal-oxide nanocomposites has been the subject of numerous studies [55]. Super oxide anions (O_2^-) and CuO-ZnO-Co3O4 nanocomposite oxidation produces Cu^{2+}, Zn^{2+}, and Co^{2+} ions, which aid in their diffusion into the biological system or cause oxidative stress and reactive oxygen species (ROS), which alter membrane permeability, harm proteins, lipids, DNA/RNA, and eventually lead to cytotoxicity in prokaryotic cells [56,57]. The more potent oxidizing agents (OH) among the ROS are hydroxyl radicals and hydrogen peroxide (H_2O_2). By directly penetrating the cell membrane of the bacteria, they damage them by preventing cell growth. Additional mechanisms are also utilized to mediate the antibacterial activity. Nanocomposite damages the bacterial cell membrane and binds to the mesosome. Due to the cell death caused by these intracellular functional changes, oxidative stress is introduced [58–60].

The negative-charged cell membranes and the heavy metal ions Cu^{2+}, Zn^{2+}, and Co^{2+} with positive charges attract each other when they come into contact with the microbe's cell membranes (Fig. 11). Cu^{2+}, Zn^{2+}, and Co^{2+} then penetrate the cell membrane and interact with the thiol groups (-SH) of the proteins that are present on the bactericidal cell surface. The proteins are rendered inactive by the nanomaterials, and the membrane permeability is reduced, which results in the microbe's death. Furthermore, the surface area of nanocomposites has a significant impact on the chemical interaction between them and the cell membrane, and the same thing happens in fungal cells [61]. We choose the most prevalent bacteria through our own process of selectivity. According to recent studies, nanocomposite exhibits greater effectiveness. While it comes to treating the most contagious strains, the treatment (Nanocomposite) is more effective than other nanoparticle because it can cure the infection effectively and efficiently [62].

4. Conclusions

The co-precipitation method was utilized to prepare pure CuO, ZnO, Co_3O_4 nanoparticles and CuO-ZnO-Co_3O_4 mixed ternary oxide nanocomposite. The XRD pattern revealed that nanocomposite has monoclinic CuO, hexagonal ZnO, and cubic Co_3O_4 structures. The

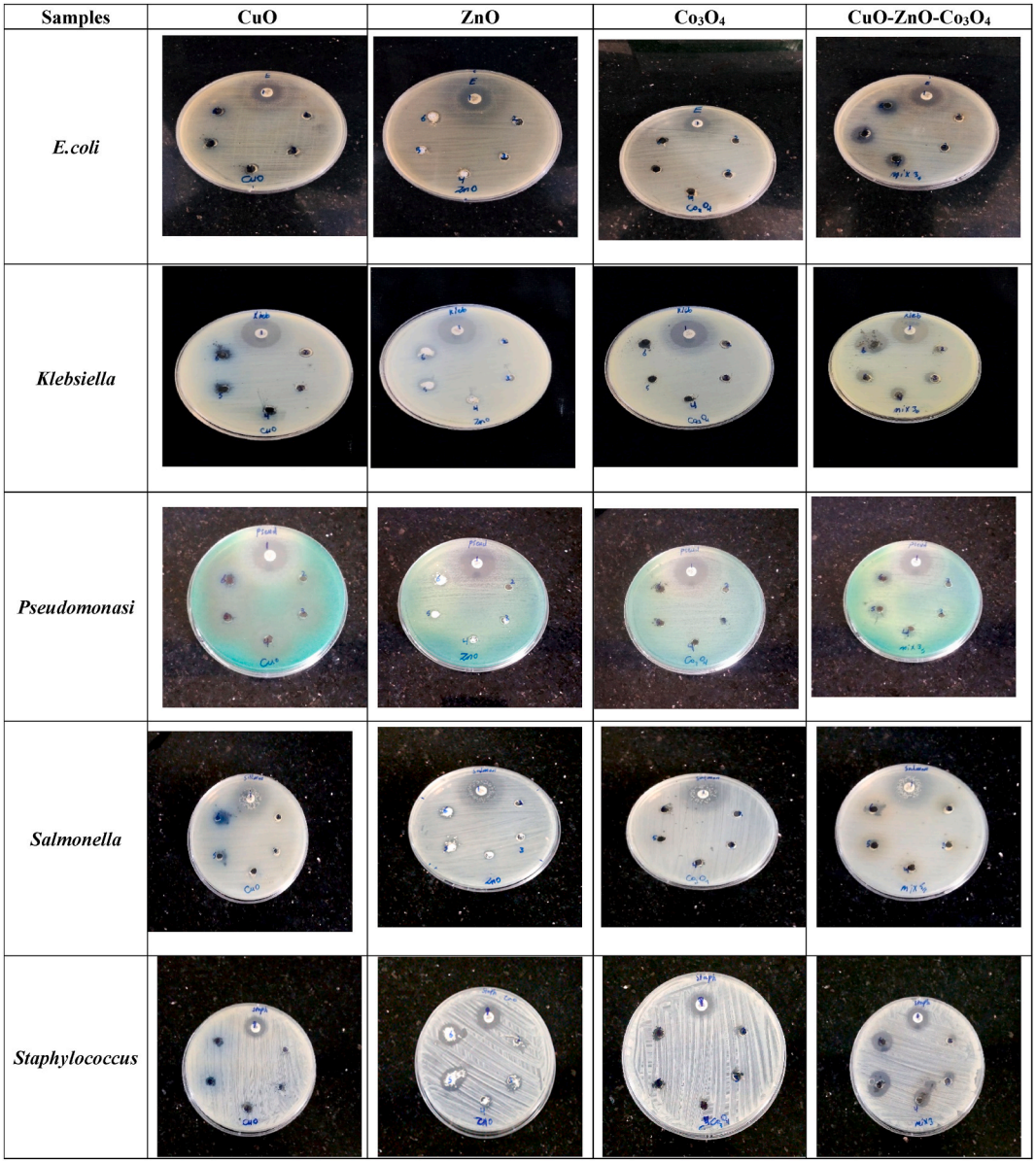

Fig. 7. Images of the CuO, ZnO, Co_3O_4 nanoparticals and CuO-ZnO-Co_3O_4 nanocomposite inhibition zones against five types of pathogenic bacterial.

nanocomposite particle size revealed by TEM image is 18.1 nm. SAED results were consistent with the indexing of XRD peaks and demonstrate the polycrystalline nature of the samples. The results of XRD were also in good agreement with TXRF results. From the results of the zeta potential, CuO nanoparticles were more stable than Co_3O_4 nanoparticles and CuO-ZnO-Co_3O_4 nanocomposite, while ZnO had poor stability. The optical band gap of nanocomposite was 1.3 eV. The antimicrobial and antifungal properties of nanocomposite are demonstrated against both Gram-positive and Gram-negative bacteria. The results showed that CuO-ZnO-Co_3O_4 nanocomposite has good antibacterial and antifungal properties. We recommend that metal oxides that we produce be applied to animals after injecting them with bacteria and fungi. Then notice the side effects and add some physical measurements, such as photocatalytic.

Data availability statement

Data will be made available on request.

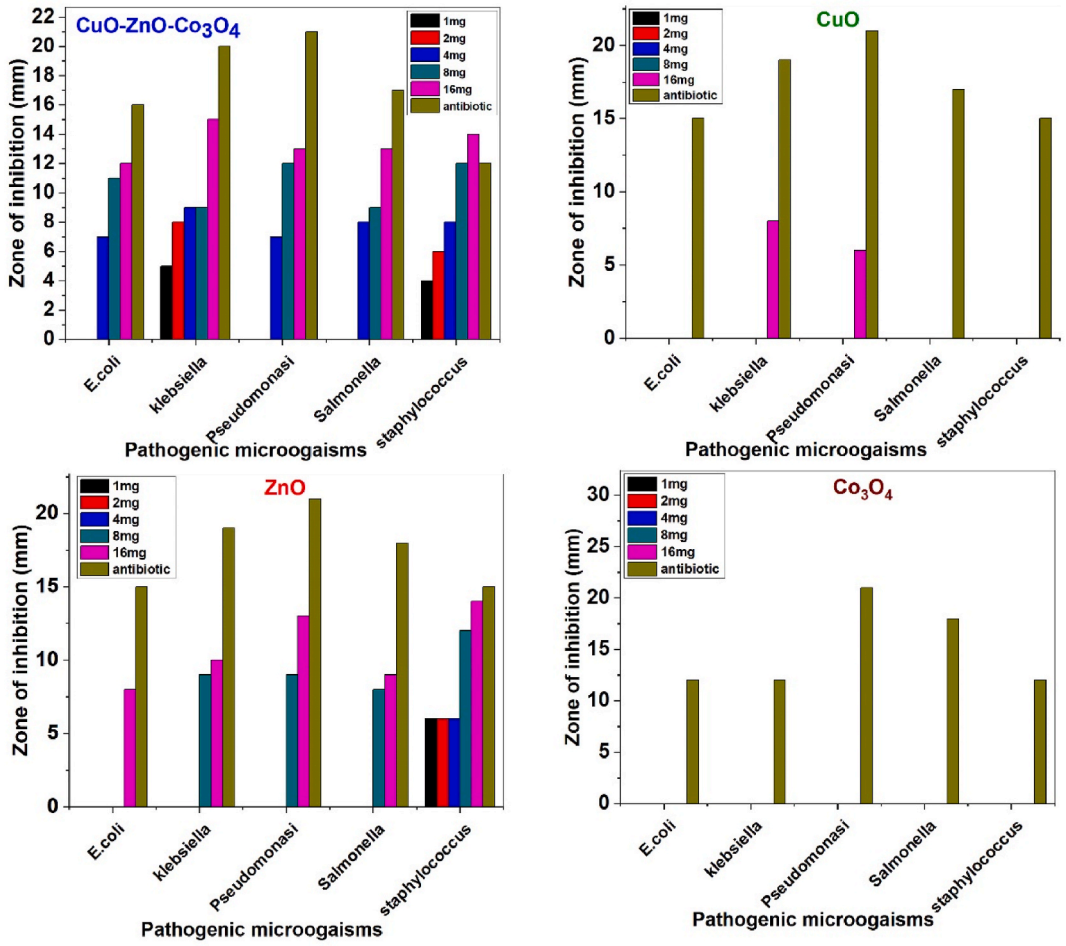

Fig. 8. Antibacterial activity of the CuO, ZnO, Co3O4 nanoparticals and CuO-ZnO-Co_3O_4 nanocomposite and an antibiotic against five types of pathogenic bacteria.

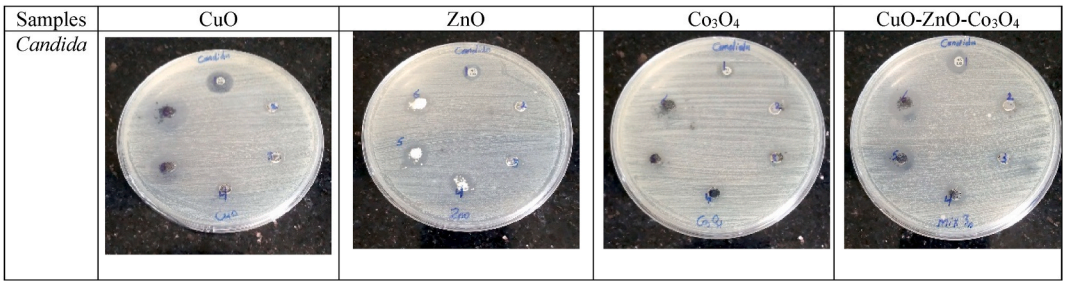

Fig. 9. Image of the CuO, ZnO, Co_3O_4 nanoparticals and CuO-ZnO-Co_3O_4 nanocomposite inhibition zones against Candida.

CRediT authorship contribution statement

Shadha Nasser Aziz: Writing – original draft, Software, Formal analysis, Data curation. **A.M. Abdulwahab:** Supervision, Software, Project administration, Methodology. **Thana Shuga Aldeen:** Writing – review & editing, Supervision, Formal analysis. **Dheyazan Mohammed Ali Alqabili:** Formal analysis.

Declaration of competing interest

The authors declare that they have no known competing financial interests or personal relationships that could have appeared to

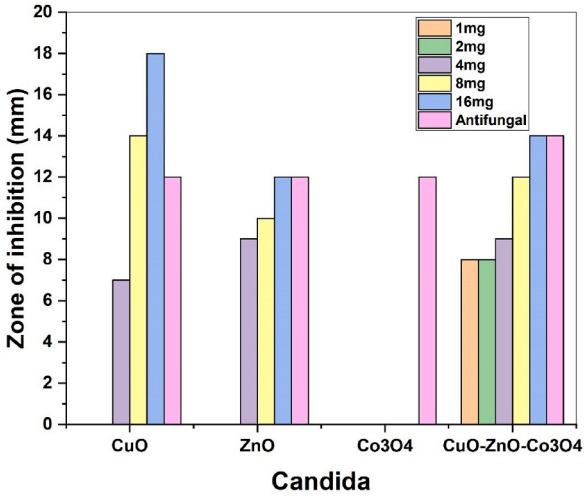

Fig. 10. Antifungal activity of the CuO, ZnO,Co_3O_4 and CuO-ZnO-Co_3O_4 nanocomposite and an antifungal against pathogenic Candida.

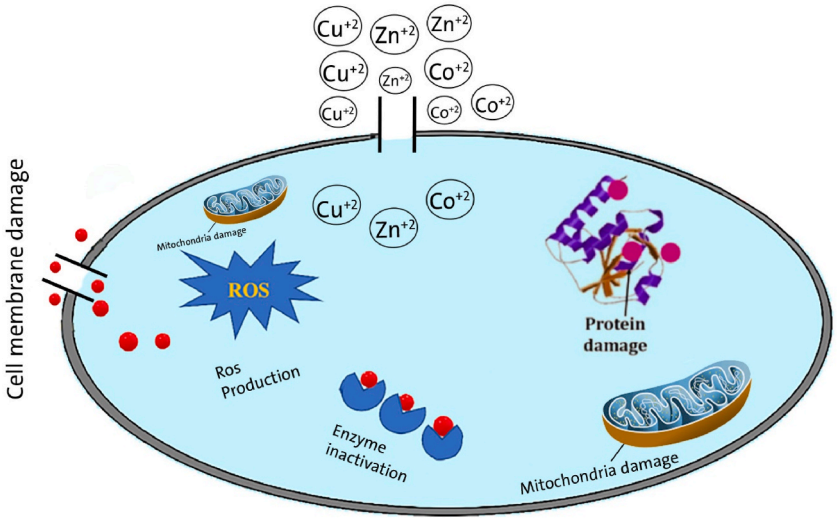

Fig. 11. Mechanism of antibacterial and antifungal activity of CuO,ZnO,Co_3O_4 nanoparticals and CuO- ZnO-Co_3O_4 nanocomposite.

influence the work reported in this paper.

Acknowledgments

The authors are grateful for Guinness University of Science and Technology, and Thamar University, Thamar city, Republic of Yemen for their support in helping us with sample processing. The authors are grateful for Dr. Majid Al-Jaradi for assisting in biological experiments. A lot of thanks for New Med Lab Specialized Laboratories and Modern Bainon Laboratory, Thamar City, Republic of Yemen.

References

[1] D.M. Yufanyi, J.F. Tendo, A.M. Ondoh, J.K. Mbadeam, CdO nanoparticles by thermal decomposition of a cadmium-hexamethylenetetramine complex, J. Mater. Sci. Res. 3 (3) (2014) 1, https://doi.org/10.5539/jmsr.v3n3p1.

[2] T. Munawar, F. Iqbal, S. Yasmeen, K. Mahmood, A. Hussain, Multi metal oxide NiO-CdO-ZnO nanocomposite–synthesis, structural, optical, electrical properties and enhanced sunlight driven photocatalytic activity, Ceram. Int. 6 (2) (2020) 2421–2437, https://doi.org/10.1016/j.ceramint.2019.09.236.

[3] N.M. Al-Hada, E.B. Saion, A.H. Shaari, M.A. Kamarudin, M.H. Flaifal, S.H. Ahmad, A. Gene, A facile thermal-treatment route to synthesize the semiconductor CdO nanoparticles and effect of calcination, Mater. Sci. Semicond. Process. 26 (2014) 460–466, https://doi.org/10.1016/j.mssp.2014.05.032.

[4] S. Balamurugan, A.R. Balu, V. Narasimman, G. Selvan, K. Usharani, J. Srivind, M. Suganya, N. Manjula, C. Rajashree, V.S. Nagarethinam, Multi metal oxide CdO–Al2O3–NiO nanocomposite—synthesis, photocatalytic and magnetic properties, Mater. Res. Express 6 (1) (2018) 015022.

[5] X. Ge, C. Ren, Y. Ding, G. Chen, X. Lu, K. Wang, F. Ren, M. Yang, Z. Wang, J. Li, X. An, B. Qian, Y. Leng, Micro/nano-structured TiO2 surface with dual-functional antibacterial effects for biomedical applications, Bioact. Mater. 4 (2019) 346–357, https://doi.org/10.1016/j.bioactmat.2019.10.006.

[6] U. Akpan, B. Hameed, The advancements in sol–gel method of doped-TiO2 photocatalysts, Appl. Catal. Gen. 375 (1) (2010) 1–11, https://doi.org/10.1016/j.apcata.2009.12.023.

[7] D. Rajesh, B.V. Lakshmi, C.S. Sunandana, Two-step synthesis and characterization of ZnO nanoparticles, Phys. B Condens. Matter 407 (23) (2012) 4537–4539, https://doi.org/10.1016/j.physb.2012.07.050.

[8] K. Karthik, S. Dhanuskodi, C. Gobinath, S. Prabukumar, S. Sivaramakrishnan, Photocatalytic and antibacterial activities of hydrothermally prepared CdO nanoparticles, J. Mater. Sci. Mater. Electron. 28 (2017) 11420–11429.

[9] V. Revathi, K. Karthik, Microwave assisted CdO–ZnO–MgO nanocomposite and its photocatalytic and antibacterial studies, J. Mater. Sci. Mater. Electron. 29 (2018) 18519–18530, https://doi.org/10.1007/s10854-018-9968-1.

[10] F. Li, H. Wang, L. Wang, J. wang, Magnetic properties of ZnFe2O4 nanoparticles produced by a low-temperature solid-state reaction method, J. Magn. Magn Mater. 309 (2) (2007) 295–299, https://doi.org/10.1016/j.jmmm.2006.07.012.

[11] S. Tazikeh, A. Akbari, A. Talebi, E. Talebi, Synthesis and characterization of tin oxide nanoparticles via the Co-precipitation method, Materials Science-Poland 32 (2014) 98–101.

[12] M. Rashad, Z.I. Zaki, H. El-Shall, A novel approach for synthesis of nanocrystalline MgAl 2 O 4 powders by co-precipitation method, J. Mater. Sci. 44 (2009) 2992–2998.

[13] G. Ren, D. Hu, E.W.C. Cheng, M.A. Reus, P. Reip, R.P. Allaker, Characterisation of copper oxide nanoparticles for antimicrobial applications, Int. J. Antimicrob. Agents 33 (6) (2009) 587–590, https://doi.org/10.1016/j.ijantimicag.2008.12.004.

[14] G. Borkow, J. Gabbay, Copper, an ancient remedy returning to fight microbial, fungal and viral infections, Curr. Chem. Biol. 3 (3) (2009) 272–278.

[15] K.R. Raghupathi, R.T. Koodali, A.C. Manna, Size-dependent bacterial growth inhibition and mechanism of antibacterial activity of zinc oxide nanoparticles, Langmuir 27 (7) (2011) 4020–4028, https://doi.org/10.1021/la104825u.

[16] G. Applerot, J. Lellouche, N. Perkas, Y. Nitzan, A. Gedanken, E. Banin, ZnO nanoparticle-coated surfaces inhibit bacterial biofilm formation and increase antibiotic susceptibility, Rsc Advances 2 (6) (2012) 2314–2321.

[17] E.P. Tan, S. Djearamane, L.S. Wong, R. Rajamani, A.C.T. Antony, S.K. Subbaih, A.K. Janakiraman, M. Aminuzzaman, V. Subramaniyan, M. Sekar, S. Selvaraj, An in vitro study of the antifungal efficacy of zinc oxide nanoparticles against Saccharomyces cerevisiae, Coatings 12 (12) (2022) 1988, https://doi.org/10.3390/coatings12121988.

[18] V. Selvanathan, M. Aminuzzaman, L.X. Tan, Y.F. Win, E.S. Cheah, M.H. Heng, L. Tey, S. Arullappan, N. Algthami, S.S. Alharthi, S. Sultana, M. Shahiduzzaman, H. Abdullah, M. Aktharuzzaman, Synthesis, characterization, and preliminary in vitro antibacterial evaluation of ZnO nanoparticles derived from soursop (Annona muricata L.) leaf extract as a green reducing agent, J. Mater. Res. Technol. 20 (2022) 2931–2941, https://doi.org/10.1016/j.jmrt.2022.08.028.

[19] G. Franci, A. Falanga, S. Galdiero, L. Palomba, M. Rai, G. Morelli, M. Galdiero, Silver nanoparticles as potential antibacterial agents, Molecules 20 (5) (2015) 8856–8874, https://doi.org/10.3390/molecules20058856.

[20] J.A. Lemire, J.J. Harrison, R.J. Turner, Antimicrobial activity of metals: mechanisms, molecular targets and applications, Nat. Rev. Microbiol. 11 (6) (2013) 371–384.

[21] R. Dadi, R. Azouani, M. Traore, C. Mielcarek, A. Kanaev, Antibacterial activity of ZnO and CuO nanoparticles against gram positive and gram negative strains, Mater. Sci. Eng. C 104 (2019) 109968, https://doi.org/10.1016/j.msec.2019.109968.

[22] P. Nagore, S. Ghotekar, K. Mane, A. Ghoti, M. Bilal, A. Roy, Structural properties and antimicrobial activities of Polyalthia longifolia leaf extract-mediated CuO nanoparticles, BioNanoScience 11 (2021) 579–589.

[23] A. Azam, A.S. Ahmed, M. Oves, M.S. Khan, S.S. Habib, A. Memic, Antimicrobial activity of metal oxide nanoparticles against Gram-positive and Gram-negative bacteria: a comparative study, Int. J. Nanomed. (2012) 6003–6009, https://doi.org/10.2147/IJN.S35347.

[24] D. Das, B.J. Saikia, Synthesis, characterization and biological applications of cobalt oxide (Co3O4) nanoparticles, Chemical Physics Impact 6 (2023) 100137, https://doi.org/10.1016/j.chphi.2022.100137.

[25] D. Sharma, J. Rajput, B.S. Kaith, M. Kaur, S. Sharma, Synthesis of ZnO nanoparticles and study of their antibacterial and antifungal properties, Thin Solid Films 519 (3) (2010) 1224–1229, https://doi.org/10.1016/j.tsf.2010.08.073.

[26] A. Khalaji, Z. Pazhand, K. Kiani, P. Machek, M. Jarosova, R. Mazandarani, CuO nanoparticles: preparation, characterization, optical properties, and antibacterial activities, J. Mater. Sci. Mater. Electron. 31 (2020) 11949–11954.

[27] S. Haq, M. Rshid, F. Menaa, N. Shahzad, M.I. Shahzad, S.Y. Alfaifi, O. Madkhali, M. Aljabri, M. Ashravi, R. Tayeb, M. Rahmani, Antibacterial and antioxidant screening applications of reduced-graphene oxide modified ternary SnO2-NiO-CuO nanocomposites, Arab. J. Chem. 16 (8) (2023) 104917, https://doi.org/10.1016/j.arabjc.2023.104917.

[28] L.F.G. Dias, G.J.C. pimentel, J.P.C. Rheinheimer, O.P. Gomes, B.G.D. Almeida, D.P. Volanti, M.T.G. Almeida, P.N. Lisboa-Filho, Synthesis and characterization of CuO-MgO-ZnO and CuO-Co3O4-CeO2, Discover Materials 3 (1) (2023) 27, https://doi.org/10.1007/s43939-023-00064-4.

[29] K. Kannan, D. Radhika, D. Gnanasangeetha, S.K. Lakkaboyana, K.K. Sadasivuni, K. Gurushankar, M.M. Hanafiah, Photocatalytic and antimicrobial properties of microwave synthesized mixed metal oxide nanocomposite, Inorg. Chem. Commun. 125 (2021) 108429, https://doi.org/10.1016/j.inoche.2020.108429.

[30] M.W. Alam, H.S. Al Qahtani, B. Souayeh, W. Ahmed, H. Albalawi, M. Farhan, A. Abuzir, S. Naeem, Novel copper-zinc-manganese ternary metal oxide nanocomposite as heterogeneous catalyst for glucose sensor and antibacterial activity, Antioxidants 11 (6) (2022) 1064, https://doi.org/10.3390/antiox11061064.

[31] L. GuzmÃ, B.S. Ramirez, C.F. Maribel, M.G. Pescador, F.J.M. Cruz, Low accuracy of the McFarland method for estimation of bacterial populations, Afr. J. Microbiol. Res. 12 (31) (2018) 736–740, https://doi.org/10.5897/AJMR2018.8893.

[32] A.M. Raba-Páez, J.O. Malafatti, C.A. Parra-Vargas, E.C. Paris, M. Rincon-Joya, Effect of tungsten doping on the structural, morphological and bactericidal properties of nanostructured CuO, PLoS One 15 (9) (2020) e0239868, https://doi.org/10.1371/journal.pone.0239868.

[33] L. Poirel, A. Jayol, P. Nordmann, Polymyxins: antibacterial activity, susceptibility testing, and resistance mechanisms encoded by plasmids or chromosomes, Clin. Microbiol. Rev. 30 (2) (2017) 557–596, https://doi.org/10.1128/cmr.00064-16.

[34] A. Wolfensberger, H. Sax, R. Weber, R. Zbinden, S. Kuster, M. Hombach, Change of antibiotic susceptibility testing guidelines from CLSI to EUCAST: influence on cumulative hospital antibiograms, PLoS One 8 (11) (2013) e79130, https://doi.org/10.1371/journal.pone.0079130.

[35] F. Paraguay-Delgado, L.A. Hermida-Montero, J.E. Morales-Mendoza, Z. Duran-Barradas, A. Mtz-Enriques, N. Parioa, Photocatalytic properties of Cu-containing ZnO nanoparticles and their antifungal activity against agriculture-pathogenic fungus, RSC Adv. 12 (16) (2022) 9898–9908.

[36] M. Sarfraz, N. Ahmed, Khizar Ul- Haq, S. Shahida, M.A. Khan, Structural optical and magnetic properties of transition metal doped ZnO magnetic nanoparticles synthesized by sol-gel auto-combustion method, Materials Science-Poland 37 (2) (2019) 280–288. http://www.materialsscience.pwr.wroc.pl/.

[37] A. Diallo, A.C. Beye, T.B. Doyle, E. Park, M. Maaza, Green synthesis of Co3O4 nanoparticles via Aspalathus linearis: physical properties, Green Chem. Lett. Rev. 8 (3–4) (2015) 30–36, https://doi.org/10.1080/17518253.2015.1082646.

[38] S. Mustapha, M.M. Ndamitso, A.S. Abdulkareem, J.O. Tijani, D.T. Shuaib, A.K. Mohammed, A. Sumaila, Comparative study of crystallite size using Williamson-Hall and Debye-Scherrer plots for ZnO nanoparticles, Adv. Nat. Sci. Nanosci. Nanotechnol. 10 (4) (2019) 045013.

[39] Y.B. Chan, M. Aminuzzaman, M.K. Rahman, Y.F. Win, S. Sultana, S. Cheah, A. Watanabe, L.S. Wong, S.K. Guha, S. Djearamane, V. Rajendran, V. Rajendran, M. Akhtaruzzaman, L. Tey, Green synthesis of ZnO nanoparticles using the mangosteen (Garcinia mangostana L.) leaf extract: comparative preliminary in vitro antibacterial study, Green Process. Synth. 13 (1) (2024) 20230251, https://doi.org/10.1515/gps-2023-0251.

[40] I.B. Miled, M. Jlassi, I. Sta, M. Dhaouadi, M. hajji, G. Mousdis, M. Kompitsas, H. Ezzaouia, Structural, optical, and electrical properties of cadmium oxide thin films prepared by sol–gel spin-coating method, J. Sol. Gel Sci. Technol. 83 (2017) 259–267.

[41] A. Alnehia, A.H. Al-Hammadi, A. Al-Sharabi, H. Alnahari, Optical, structural and morphological properties of ZnO and Fe+ 3 doped ZnO-NPs prepared by Foeniculum vulgare extract as capping agent for optoelectronic applications, Inorg. Chem. Commun. 143 (2022) 109699, https://doi.org/10.1016/j.inoche.2022.109699.

[42] A. Al-Sharabi, K.S.S. Sada'a, A. AL-Osta, R. Abd-Shukor, Structure, optical properties and antimicrobial activities of MgO–Bi2− x Cr x O3 nanocomposites prepared via solvent-deficient method, Sci. Rep. 12 (1) (2022) 10647, https://doi.org/10.1038/s41598-022-14811-9.
[43] M. Ishfaq, W. Hassan, M. Sabir, H.H. Somaily, S.K. Hachim, Z.J. Kadhim, H.A. Lafta, Y.S. Alnassar, A.M. Rheima, S.R. Ejaz, M. Aadil, Wet-chemical synthesis of ZnO/CdO/CeO2 heterostructure: a novel material for environmental remediation application, Ceram. Int. 48 (23) (2022) 34590–34601, https://doi.org/10.1016/j.ceramint.2022.08.046.
[44] M.A. Qamar, S. Shahid, M. Javed, S. Iqbal, M. Sher, M.B. Akbar, Highly efficient g-C3N4/Cr-ZnO nanocomposites with superior photocatalytic and antibacterial activity, J. Photochem. Photobiol. Chem. 401 (2020) 112776, https://doi.org/10.1016/j.jphotochem.2020.112776.
[45] T. Parsai, A. Kumar, Stability and characterization of mixture of three particle system containing ZnO-CuO nanoparticles and clay, Sci. Total Environ. 740 (2020) 140095, https://doi.org/10.1016/j.scitotenv.2020.140095.
[46] P. Sati, R.C. Shenda, S. Ramaprabhu, An experimental study on thermal conductivity enhancement of DI water-EG based ZnO (CuO)/graphene wrapped carbon nanotubes nanofluids, Thermochim. Acta 666 (2018) 75–81, https://doi.org/10.1016/j.tca.2018.06.008.
[47] R. Henderson, S.A. Parsons, B. Jefferson, Successful removal of algae through the control of zeta potential, Separ. Sci. Technol. 43 (7) (2008) 1653–1666, https://doi.org/10.1080/01496390801973771.
[48] I. Khan, I. Khan, M. Usman, M. Imran, K. Saeed, Nanoclay-mediated photocatalytic activity enhancement of copper oxide nanoparticles for enhanced methyl orange photodegradation, J. Mater. Sci. Mater. Electron. 31 (2020) 8971–8985, https://doi.org/10.1007/s10854-020-03431-6.
[49] O.N. Hussein, S.M.H. AL-Jawad, Natheer, Efficient antibacterial activity enhancement in Fe/Mn co-doped CuS nanoflowers and nanosponges, Bull. Mater. Sci. 46 (3) (2023) 139, https://doi.org/10.1007/s12034-023-02964-w.
[50] T.S. Aldeen, H.E.A. Mohamed, M. Maaza, ZnO nanoparticles prepared via a green synthesis approach: physical properties, photocatalytic and antibacterial activity, J. Phys. Chem. Solid. 160 (2022) 110313, https://doi.org/10.1016/j.jpcs.2021.110313.
[51] S. Al-Ariki, N.A.A. Yahya, S.A. Al-A'nsi, M.H.H. Jumali, A.N. Jannah, R. Abd-Shukor, Synthesis and comparative study on the structural and optical properties of ZnO doped with Ni and Ag nanopowders fabricated by sol gel technique, Sci. Rep. 11 (1) (2021) 11948, https://doi.org/10.1038/s41598-021-91439-1.
[52] S.A. Makhlouf, Z.H. Bakr, K.I. Aly, M.S. Moustafa, Structural, electrical and optical properties of Co3O4 nanoparticles, Superlattice. Microst. 64 (2013) 107–117.
[53] A. Abdulwahab, A.A. AL-Adhreai, A.A.A. Ahmed, Influence of Ni-Co dual doping on structural and optical properties of CdSe thin films prepared by chemical bath deposition method, Optik 236 (2021) 166659, https://doi.org/10.1016/j.ijleo.2021.166659.
[54] J.T. Wright, D. Su, T.V. Buuren, R.W. Meulenberg, Electronic structure of cobalt doped CdSe quantum dots using soft X-ray spectroscopy, J. Mater. Chem. C 2 (39) (2014) 8313–8321.
[55] A.A. Ezhilarasi, J.J. Vijaya, K. Kaviyarasu, M. Maaza, A. Ayeshamariam, L. J Kennedy, Green synthesis of NiO nanoparticles using Moringa oleifera extract and their biomedical applications: cytotoxicity effect of nanoparticles against HT-29 cancer cells, J. Photochem. Photobiol. B Biol. 164 (2016) 352–360, https://doi.org/10.1016/j.jphotobiol.2016.10.003.
[56] H. Zulfiqar, A. Zafar, M.N. Rasheed, Z. Ali, K. Mehmood, A. Mazher, M. Hasan, N. Mahmooed, Synthesis of silver nanoparticles using Fagonia cretica and their antimicrobial activities, Nanoscale Adv. 1 (5) (2019) 1707–1713.
[57] M. Hasan, M. Altaf, A. Zafar, S.G. Hassan, Z. Ali, G. Mustafa, T. Munawar, M.S. Saif, T. Tariq, F. Iqbal, M.W. Khan, A. Mahmood, N. Mahmmod, X. Shu, Bioinspired synthesis of zinc oxide nano-flowers: a surface enhanced antibacterial and harvesting efficiency, Mater. Sci. Eng. C (2021) 111280, https://doi.org/10.1016/j.msec.2020.111280.
[58] K. Karthik, S. Dhanuskodi, C. Gobinath, S. Prabukumar, S. Sivaramakrishnan, Multifunctional properties of microwave assisted CdO–NiO–ZnO mixed metal oxide nanocomposite: enhanced photocatalytic and antibacterial activities, J. Mater. Sci. Mater. Electron. 29 (2018) 5459–5471, https://doi.org/10.1007/s10854-017-8513-y.
[59] A.A. Al-Mushki, A.A.A. Ahmed, A.M. Abdulwahab, S.A.S. Qaid, N.S. Alzayed, M. Shahabuddin, J.M. Abduljalil, F.A.A. Saad, Effect of the molar ratio of (Ni2+ and Fe3+) on the magnetic, optical and antibacterial properties of ternary metal oxide Cdo–Nio–Fe2o3 nanocomposites, Sci. Rep. 13 (1) (2023) 9021, https://doi.org/10.1038/s41598-023-36262-6.
[60] A.A.A. Ahmed, A.A.A. AL-Mushki, B.A. AL-Asbahi, A.M. Abdulwahab, J.M.A. Abduljalil, F.A.A. Saad, S.M.H. Qaid, H.M. Ghaithan, W.A. Farooq, A. Omar, Effect of ethylene glycol concentration on the structural and optical properties of multimetal oxide CdO–NiO–Fe2O3 nanocomposites for antibacterial activity, J. Phys. Chem. Solid. 155 (2021) 110113, https://doi.org/10.1016/j.jpcs.2021.110113.
[61] R. Zhang, Y. Cui, M. Cheng, Y. Guo, X. Wang, J. Wang, Antifungal activity and mechanism of cinnamon essential oil loaded into mesoporous silica nanoparticles, Ind. Crop. Prod. 171 (2021) 113846, https://doi.org/10.1016/j.indcrop.2021.113846.
[62] S. Qasim, A. Zafar, M.S. Saif, Z. Ali, M. Nazar, M. Waqas, T. Tariq, S.G. Hassan, F. Iqbal, X. Shu, M. Hasan, Green synthesis of iron oxide nanorods using Withania coagulans extract improved photocatalytic degradation and antimicrobial activity, J. Photochem. Photobiol. B Biol. 204 (2020) 111784, https://doi.org/10.1016/j.jphotobiol.2020.111784.